Asian Journal of Civil Engineering (2023) 24:919–935
https://doi.org/10.1007/s42107-022-00548-3

ORIGINAL PAPER

A study on the near and far-field earthquake response of a low and mid-rise building resting on soft soil considering soil–structure interaction (SSI)

Sajjad Golafshani[1] · Ali Akhtarpour[1] · Hoda Ghaemi Rad[1] · Sajjad Khosravi[1,2]

Received: 16 February 2022 / Accepted: 30 November 2022 / Published online: 8 December 2022

Abstract
In this paper, the seismic performance of a low and mid-rise moment-resisting steel frame has been studied, including three and nine stories buildings with a mat foundation on soft soil, under the near and far-field earthquake effects through two-dimensional modeling using the FDM. The frames mentioned above were analyzed under fixed-base (no SSI) and flexible-base (considering SSI) conditions. Results show that the near-field earthquake imposed more critical responses than the far-field earthquake, indicating the importance of investigating near-filed earthquakes. In addition, it is observed that soil–structure interaction (SSI) increases stress and amplitude compared to a fixed base.

Keywords Near-field · Far-field · Soil–structure interaction · FLAC · Low and mid-rise building · Soft soil

Introduction

Past studies show that near and far-field earthquake records significantly differ depending on earthquake characteristics (Adanur et al., 2012; Bray & Rodriguez-Marek, 2004; Cao & Ronagh, 2014; Chopra & Chintanapakdee, 2001; Somerville, 2003; Zhang & Wang, 2013), and various buildings have been studied under different excitation by many researchers (Bhandari et al., 2019; Failed, 2018; Sharma et al., 2020). For single-degree freedom systems, the near-field earthquake imposes a greater strength demand than the far-field earthquake (Chopra & Chintanapakdee, 2001). Davoodi et al., by studying an embankment dam, show that the far-field earthquake resulted in input energy more gradually to the dam over more cycles (Davoodi et al., 2013). The effect of forwarding directivity (pulse) ground motions on tunnel-form buildings (TFB) was explained and resulted in TFBs being more vulnerable when subjected to near-field earthquakes, especially for taller constructions (Behesthi Aval et al., 2018). Near-field earthquakes for masonry structures resulted in higher displacement (Bilgin & Hysenlliu, 2019). Fragility analysis of arched hydraulic tunnels revealed that near-field earthquakes cause more significant deformations (Xie & Sun, 2021). Abd-Elhamed et al. investigate the performance of a structure with a tuned mass damper (TMD), and the results show a considerable increase in the dissipated amount of damping energy (Abd-Elhamed & Mahmoud, 2019). The study, analysis, and risk assessment of structures always interest researchers (Sharma et al., 2018; Sharma et al., 2021, 2022a, 2022b). Sharma et al. analyzed a ten-story frame and showed that a high directivity ratio affects the probability of exceedance (Sharma et al., 2021b). The structure's response is affected by parameters such as energy dissipation (Sharma et al., 2019, 2021). This concept attracted much attention after the Kobe (1995) and North (1994) earthquakes. Sharma et al. studied the response of S.R. frame under various far and near-field earthquakes. They found a significant effect of energy dissipation at the connection of S.R. frames, which improves the inelastic response of mentioned frame compared to the rigid frame (Sharma et al., 2019).

✉ Ali Akhtarpour
akhtarpour@um.ac.ir

Hoda Ghaemi Rad
hodarad7496@gmail.com

Sajjad Khosravi
geo.sajad.406@gmail.com

[1] Department of Civil Engineering, Faculty of Engineering, Ferdowsi University of Mashhad, Mashhad, Azadi Sq., Khorasan Razavi, Iran

[2] School of Civil Engineering, Iran University of Science & Technology, Tehran, Iran

Sehhati et al. concluded that compared to forward-directivity ground motions, the mean seismic responses of steel moment frame buildings and their dispersion are more significant for far-fault ground motions (Sehhati et al., 2011). Gerami et al. showed that the structures subjected to near-field earthquakes tend to oscillate primarily in the first vibration mode. (Gerami & Abdollahzadeh, 2015). Mashayekhi et al. showed that the higher-mode effects under far-field earthquakes are more significant (Mashayekhi et al., 2019). Mansouri concluded that floor displacements, inter-story drift ratios, and story shears induced by near-field earthquakes are significantly greater than far-field earthquakes (Mansouri et al., 2019). Zomorodian et al. concluded that dense sand is the most reliable soil, while soft clay is the most critical (Zomorodian et al., 2021). The study on the lateral drift of the self-centering beam for steel moment-frames shows that all of the SCB-MFs, experienced an evident increase in the inter-story drift demand as the excitation was changed from the F.F. and N.P. to the N.F. records (Huang et al., 2021).

The dynamic structural response depends on soil-foundation-structure interactions. Usually, structures are modeled under fixed base conditions (Sharma et al., 2019, 2021a, 2021b). While, in reality, oscillation energy transfers through underlying soil to the base, which causes foundations to interact with the supporting system justifying to use of soil–structure systems instead of rigid base systems (Dutta et al., 2004). Taking the interaction between the structure and base under earthquakes into consideration is more important than being ignored. SFSI[1] has attracted the attention of researchers during past decades (Gerami & Abdollahzadeh, 2015; Sehhati et al., 2011). Interaction affects the foundation displacement amplitude depending on the frequency of seismic waves (Elwi et al., 2018). SFSI decreases the structural system's stiffness and increases the natural period, and displacements for upper stories are significantly affected by SFSI (Dutta et al., 2004; Khazaei et al., 2017; Stewart et al., 1999). Therefore, considering SFSI for high-rise buildings significantly affects the response (Avilés & Pérez-Rocha, 1998). Researches show that SSI affects the response of low-rise buildings (steel frames) on dense silty sand (Raychowdhury, 2009). Güllü et al. investigated SSI and fixed-base consideration on a relatively complex historical stone masonry mosque, showing that the effects of the SSI in both the near and far-field earthquakes amplified the displacement, velocity, acceleration, and stresses on the building (Güllü & Karabekmez, 2017).

In this research, an investigation has been performed to study the seismic performance of a Low and Mid-rise steel moment-resisting frame, including 3- and 9-story buildings with a mat foundation on a soft soil deposit, under the near and far-fault earthquake effects through 2D modeling using the FDM software package of FLAC. The frames as mentioned above were analyzed under two different boundary conditions: (1) fixed-base (no soil–structure interaction) and (2) flexible-base (considering soil–structure interaction). The results of the analyses in terms of structural forces and lateral displacements for the boundary as mentioned above conditions are compared and discussed. In this research, non-linear properties of soil and steel materials have been used. This study employed a direct method to model the entire soil–structure system in a single step. FLAC 2D is used to analyze soil and structure behavior simultaneously (Itasca Consulting Group & Inc, 2019; Kramer, 1996).

[1] Soil–foundation–structure interaction.

Model definition

FLAC used various elements for modeling, including beam elements, soil medium, boundaries, quiet boundaries, and interface elements, as shown in Fig. 1.

In this study, inelastic structural analysis has been used. An inelastic analysis follows a similar process to general linear analysis in which engineers create a building or structure model subjected to the desired motions. The main difference is including a plastic moment in addition to elastic properties in model components (Reza Tabatabaiefar & Fatahi, 2014). In this paper, inelastic bending is simulated by specifying a limiting plastic moment, the Mohr–Coulomb failure criterion shown in Fig. 2 chosen as a constitutive model [implemented by past research (Conniff & Kiousis, 2007; Rayhani & Naggar, 2008; Reza Tabatabaiefar & Fatahi, 2014; Zomorodian et al., 2021)], and element sizes in this paper have been chosen according to Kuhlemeyer and Lysmer (Kuhlemeyer & Lysmer, 1973). According to previous studies (Comartin et al., 1996; Council, 2003; Rayhani & Naggar, 2008), in this paper, the depth and width of the model are assumed to be 30 and 200 m, respectively (five times the width of the structure).

Simulation process

System characteristics

In this study, three and nine-story buildings selected from SAC project models (Ohtori et al., 2004) have been selected in conjunction with Bangkok Clay. The characteristics of the frames are summarized in Table 1.

Selected sections are wide flange, and the specifications of the steel sections used in the three-story and nine-story structures are shown in Figs. 3 and 4, respectively.

Characteristics of soils are shown in Table 2. Groundwater is assumed to be at the ground level; thus, the soil is saturated.

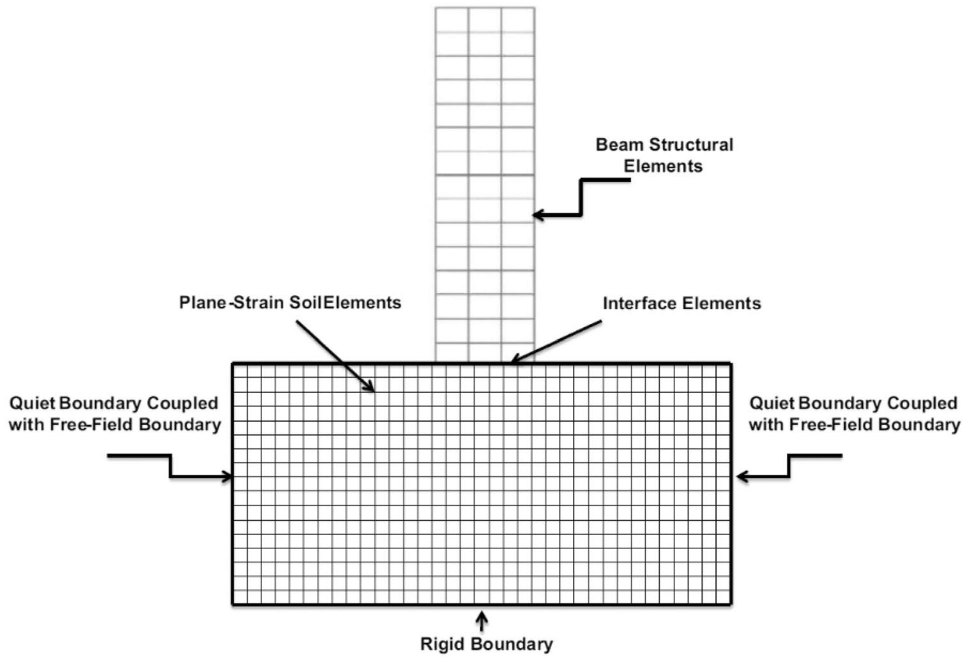

Fig. 1 Components of the soil–structure model in FLAC two-dimensional (Reza Tabatabaiefar & Fatahi, 2014)

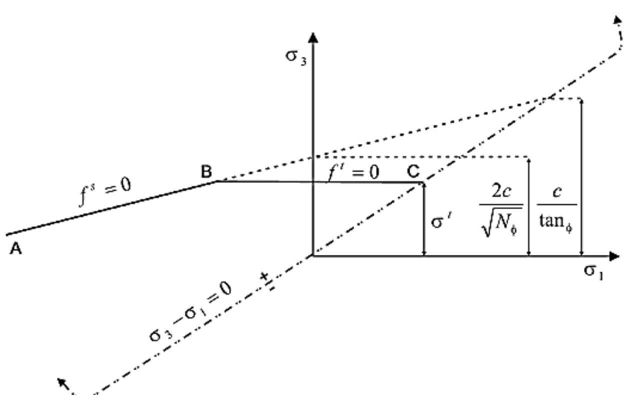

Fig. 2 Mohr–Coulomb failure criterion (Itasca Consulting Group & Inc, 2019)

Table 1 Dimensional characteristics of the studied frames

Reference name	Number of stories	Number of bays	Story height (m)	Bay width (m)	Total width (m)
S3	3	4	4	9	36
S9	9	5	4	9	45

Near and far fault earthquake acceleration utilized in the time-history analysis tabulated in Tables 3 and 4. Selected acceleration is bedrock records and downloaded from the PEER website. Response spectra for far and near-field motion are depicted in Figs.5 and 6, respectively (Peer Ground Motion Data Base, 2022).

In this study, the Hardin model, as dictated in Eq. 1 (Hardin & Drnevich, 1972), is employed among the functions in FLAC to implement hysteretic damping with 2% local damping to remove residual oscillations without affecting the solution time step.

$$M_s = \frac{1}{1 + \gamma/\gamma_{ref}} \quad (1)$$

where M_s is the secant modulus (G/G_{max}), γ is the cyclic shear strain, and γ_{ref} is Hardin/Drnevich constant. In this study, $\gamma_{ref} = 0.234$ representing the backbone curves suggested by Sun et al. (Sun et al., 1988) for clay is adopted. Figure 7 illustrates the adopted backbone curves in this study.

Numerical analysis results

In this study, dynamic analysis is performed for three and nine-story models under fixed-base conditions and considering subsoil using the direct method of SSI.

Base shear is the total lateral force or shear at the base level where the ground motion is assumed to be transmitted to the structure. The base shear at the specified points, which are shown in Figs. 8 and 9 are calculated for three-story and nine-story models, respectively. The base shear values are calculated and averaged during implemented earthquakes. The results are shown in Figs. 10, 11, 12 and 13 maximum absolute values for each model are presented in Table 5. Based on Figs. 10, 11, 12 and 13, it is found that due to pulse impact effects of near-fault, at any time, the base shear

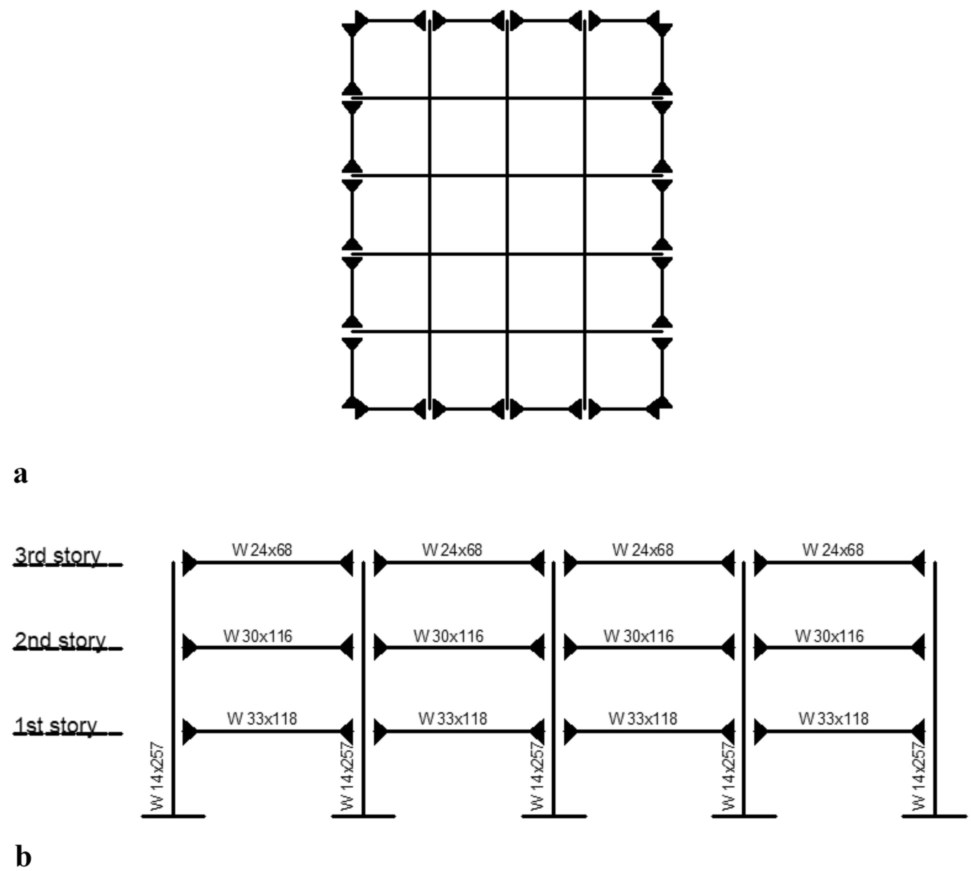

Fig. 3 Three-story structure: **a** plan of three-story structure, **b** specifications of the investigated 3-story structure (Ohtori et al., 2004)

value of the near-fault is greater than the far fault and should be considered in the seismic design of the structure. Considering fixed base leads to a higher shear base compared to the flexible base for near-field motion while it will not significantly affect base shear for the far-field earthquake. High-rise buildings (i.e., nine-story structures) lead to higher shear base results than low-rise structures, which is much more significant for near-field than far-field earthquakes.

The horizontal acceleration is the acceleration generated by the applied seismic load at each level of the structure. This study shows the horizontal acceleration for near and far fault earthquakes at the specified points in Figs. 14 and 15 is calculated for three-story and nine-story models, respectively, and the maximum value is selected. The results are shown in Figs. 16, 17, 18 and 19 and are tabulated in Tables 6, 7, 8 and 9. The results of the observations obtained are as follows.

In flexible base models (models 1, 2, 3, 4), the maximum horizontal acceleration at the bedrock level is the same for both near-fault and far-fault earthquakes, and the acceleration at the base after moving through the soil layer is 70 percent higher than at the bedrock level. Maximum horizontal acceleration in fixed-base models is less than that of flexible models at each level, which shows the importance of soil–structure interaction existence. The maximum horizontal acceleration values increase as the number of floors increases. The horizontal acceleration of near-fault is higher than far-fault earthquakes at each level of structure.

The maximum absolute displacements of all structural floors under all earthquake records are averaged. Average floor displacement for the investigated models shown in Figs. 20, 21, 22 and 23. As shown in Figs. 20, 21, 22 and 23, the displacement of floors increases with increasing floor height. However, the rate of increase in displacement on the lower floors is more significant on the upper floors due to the p-delta effect. As can be seen, due to the near-fault earthquake's pulse impact, the displacement of floors under near-fault earthquakes is higher than that of under-far-fault earthquakes. Additionally, the displacement of floors in fixed-base models is less than that of flexible models at each level, indicating the importance of soil–structure interaction. Nine-story buildings also lead to higher relative displacement than three-story.

Figures 24, 25, 26 and 27 show the average drift ratio of structural floors. As shown in the following figures, the drift ratios are higher on the first floors of the structure, and the average story drift ratio of near-fault is higher than far-faults earthquakes at each level of the structure.

In designing a structure, settlement of the foundation is an essential factor, especially when considering the SSI.

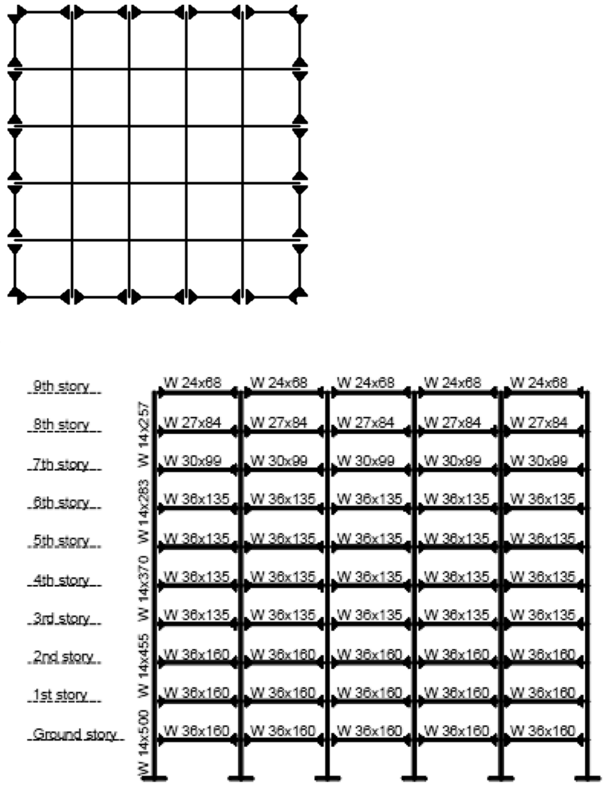

Fig. 4 Nine-story structure: **a** plan of nine-story structure, **b** specifications of the investigated 9-story structure (Ohtori et al., 2004)

For this purpose, the differential settlement values for the two points are shown in Figs. 28 and 29 are examined, and the settlement values are expressed in Table 9. Table 10 shows settlement values are higher for near-faults than far-field earthquakes for both three- and nine-story flexible bases. Also, it is found that the increase in stresses in the subsoil and considered soil behavior caused the differential settlement of nine stories to be higher compared to three stories. It must be noted that uniform settlement does not lead to stress in the structure. The main problem is the differential settlement and its effect on changing the values of internal forces of structural members. Therefore, studying the bending moments and shear forces created by earthquakes in frame beams and columns is necessary.

Each applied earthquake causes bending moments at specified points, shown in Figs. 30 and 31 are extracted then the maximum values are selected. As seen in Figs. 32, 33, 34 and 35, the bending moment values decrease with the increasing number of floors with a decreasing trend. The maximum bending moments of near-fault are higher than the far-faults earthquakes at each level of structure. Furthermore, comparing flexible base models and fixed-base models shows that SSI increases the bending moment

Table 2 Geotechnical characteristics of the adopted soil in this study

Saturated unit-weight (kg/m^3) (Likitlersuang et al., 2013)	Shear wave velocity V_s (m/s) (Warnitchai et al., 2000)	C' (kPa) (Surarak et al., 2012)	φ' (deg) (Surarak et al., 2012)	ψ' (deg) (Surarak et al., 2012)	E_{50}^{ref} (kPa) (Surarak et al., 2012)	Poisson's ratio (ν) (Surarak et al., 2012)	Moisture content (%) (Surarak et al., 2012)	Thickness (m)
2100	200–260	11.5	28	0	9500	0.25	23	30

Table 3 Near fault acceleration used in this study

Earthquake	Station	R_{JB} (km)	R_{Rup} (km)	V_{s30} (m/s)	Mw (R)	Fault mechanism	PGA (m/s^2)
Tabas (1978)	Tabas	1.79	2.05	767	7.35	Re[a]	0.86
Loma Prieta (1989)	Los Gatos	3.22	5.02	1070	6.93	Re/Ob[b]	0.44
Landers (1992)	Lucerne	2.19	2.19	1369	7.28	SS[c]	0.73
Chi Chi (1999)	TCU102	1.49	1.49	715	7.62	Re/Ob	0.30
Kocaeli (1999)	Gebze	7.57	10.92	792	7.51	SS	0.26
Kocaeli (1999)	Izmit	3.62	7.21	811	7.51	SS	0.23
L'Aquila (2009)	L'Aquila-Parking	1.3	5.38	717	6.30	No[d]	0.33

[a]Reverse

[b]Reverse oblique

[c]Strike slip

[d]Normal

Table 4 Far fault acceleration used in this study

Earthquake	Station	R_{JB} (km)	R_{Rup} (km)	V_{s30} (m/s)	Mw (R)	Fault mechanism	PGA (m/s^2)
San Fernando (1971)	Pasadena-Old Seismo Lab	21.5	21.5	969	6.61	Re	0.2
Morgan Hill (1984)	Gilroy-Gavilan Coll	14.83	14.85	730	6.19	SS	0.12
Morgan Hill (1984)	Gilroy array #1	14.90	14.91	1428	6.19	Re	0.098
Loma Prieta (1989)	UCSC	12.15	18.51	713	6.93	Re/Ob	0.40
Loma Prieta (1989)	UCSC Lick Observatory	12.04	18.41	714	6.93	Re/Ob	0.42
Northridge-01 (1994)	L.A.—Wonderland Ave	15.11	20.29	1222	6.69	Re	0.16
Northridge-01 (1994)	Vasquez Rocks Park	23.1	23.64	997	6.69	Re	0.15
Iwate-Japan (2008)	IWT010	16.26	16.27	826	6.90	Re	0.29

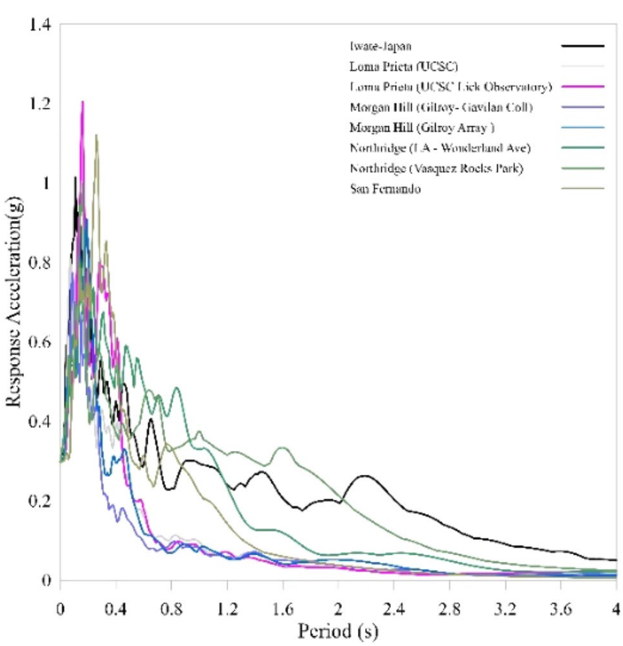

Fig. 5 Response spectra of far-field motion (Peer Ground Motion Data Base, 2022)

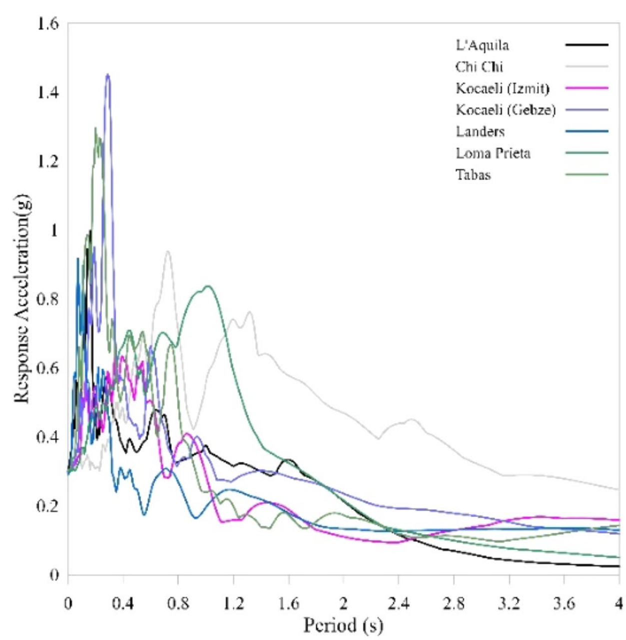

Fig. 6 Response spectra of near-field motion (Peer Ground Motion Data Base, 2022)

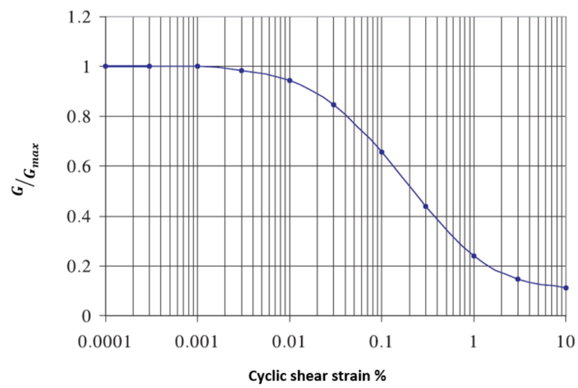

Fig. 7 Relations between $G/G_{\max}$ versus cyclic shear strain (Sun et al., 1988)

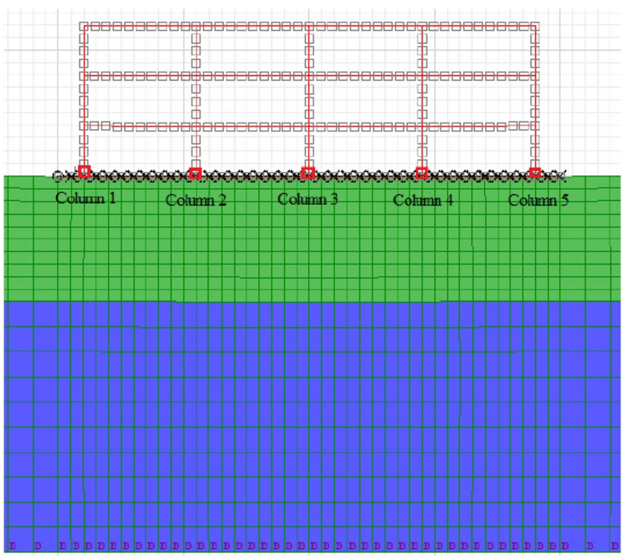

Fig. 8 Specified points of three-story models position to calculate the base shear of columns (models 1, 2, 5, 6)

considerably, and high-rise building leads to higher values of the maximum bending moment than low-rise building.

Figures 36, 37, 38 and 39 show the Shear force of the specified structure points, shown in Figs. 8 and 9, versus the structural floors under applied motions. As shown in Figs. 36, 37, 38 and 39, the values of shear forces decrease as the number of floors increases, so the diagrams have a downward trend. According to the diagram, the Shear force of near-fault earthquakes is higher than the earthquakes far from faults at each level of structure, and the nine-story building has higher shear values than the three-story building. In other words, the changes and effects of shear force are similar to the maximum bending moment.

Figures 40, 41, 42, 43, 44, 45 and 46 Show the average axial force of the lateral and middle columns of the structure. Maximum axial force values are higher for near-fault than

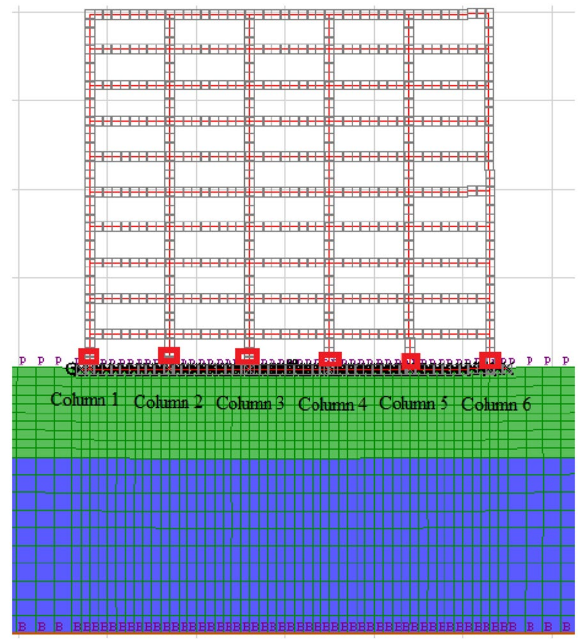

Fig. 9 Specified points of nine-story models position to calculate the base shear of columns (models 3, 4)

far-fault earthquakes because of the pulse impact effect of near-fault earthquakes. Furthermore, it can be seen that the maximum values of axial force caused by near-fault and far-fault earthquakes in lateral columns of structures have more considerable differences than those in middle columns due to the low axial load of side columns and the impact pulse effect of near-fault earthquakes. According to the analysis results, the minimum values of axial force in lateral and middle columns and for the average value of the columns are less in near-fault earthquakes than in far-fault earthquakes because of the uplift columns, which should be considered in the design. Furthermore, comparing flexible base models and fixed-base models shows that SSI increases the maximum axial force of columns and decreases the minimum axial force considerably.

Conclusions

In this paper, dynamic soil–structure interaction simulates to determine the inelastic seismic response for three and nine-story structures considering fixed and flexible bases excitation by various near and far-field ground motions. Base shear due to near-field motion has a greater value than far-field because of the pulse impact effects of near-fault. Changing the foundation from flexible to fixed-base will also increase the shear base results for near-field earthquakes, while it will not significantly be affected by far-field earthquakes. In addition, maximum horizontal acceleration, relative

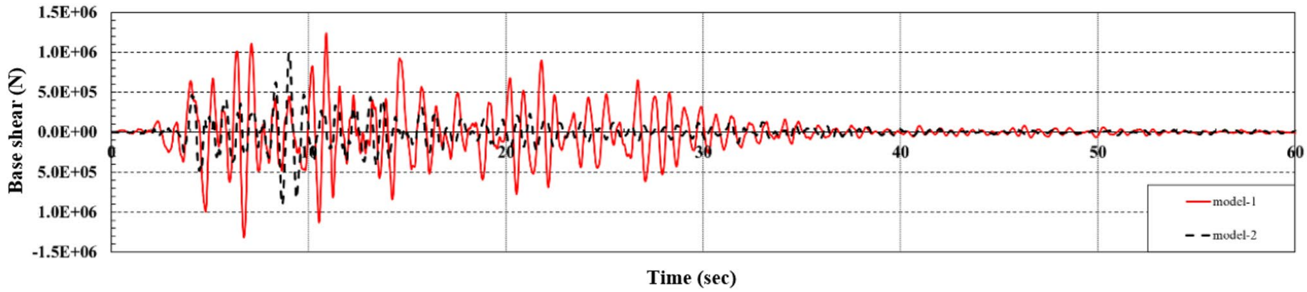

Fig. 10 Base shear values of three-story flexible base models (model 1 and model 2)

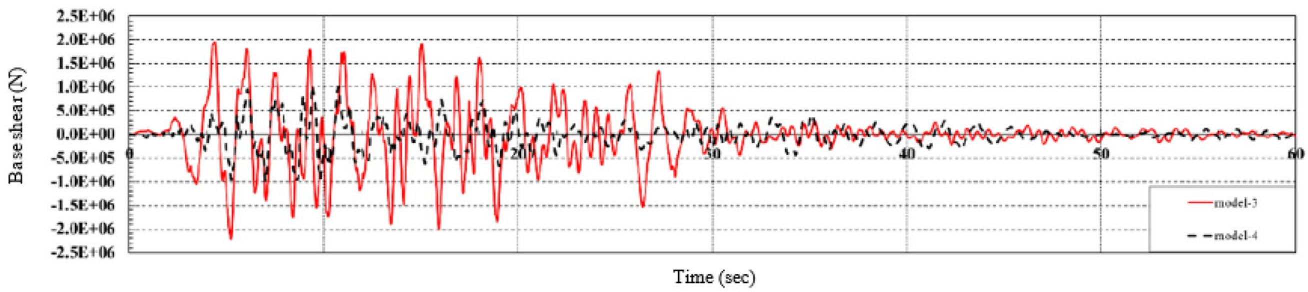

Fig. 11 Base shear values of nine-story flexible base models (model 3 and model 4)

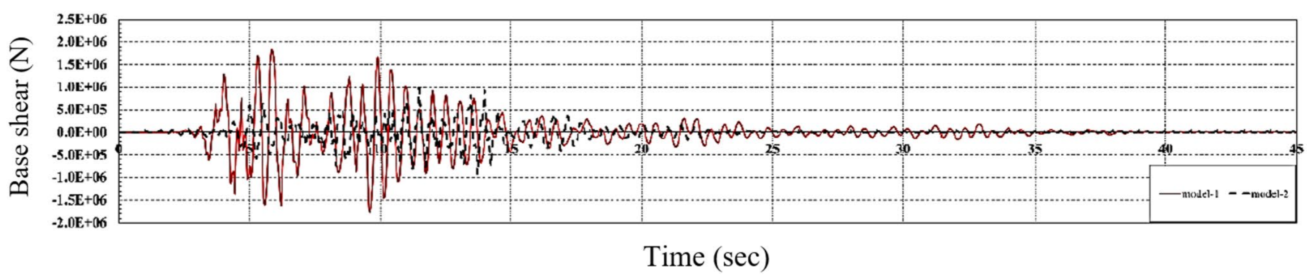

Fig. 12 Base shear values of three-story fixed-base models (model 5 and model 6)

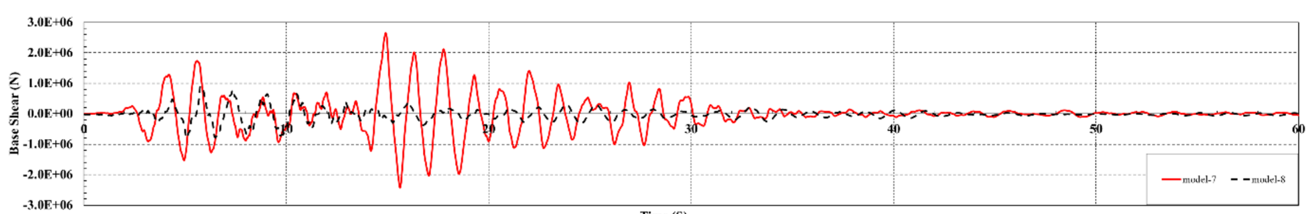

Fig. 13 Base shear values of nine-story fixed-base models (model 7 and model 8)

displacement, drift ratio, settlement, maximum bending moment, shear force, and maximum axial force are higher for near-field than far-field excitation. The fixed base showed a lower maximum horizontal acceleration, axial force, relative displacement, and maximum bending moment at each level than the flexible base, which indicates soil–structure interaction importance. Drift ratio as a parameter for damage assessment has a higher value for the first floors.

Table 5 Comparison of maximum base shear in all models

	Seismic type	Model number	Base shear (kN)
Three-story flexible-base models	Near fault	Model 1	1240.810
	Far fault	Model 2	989.330
Nine-story flexible-base models	Near fault	Model 3	1956.990
	Far fault	Model 4	1042.120
Three-story fixed-base models	Near fault	Model 5	1828.028
	Far fault	Model 6	976.942
Nine-story fixed-base models	Near fault	Model 7	2649.942
	Far fault	Model 8	909.815

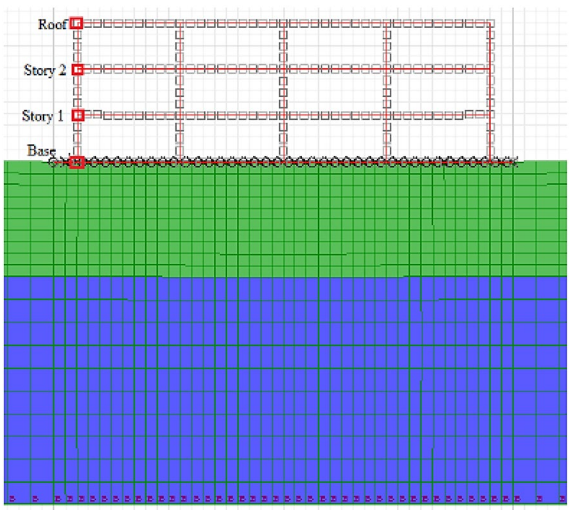

Fig. 14 Specified points of three-story models Position to calculate the maximum horizontal acceleration (models 1, 2, 5, 6)

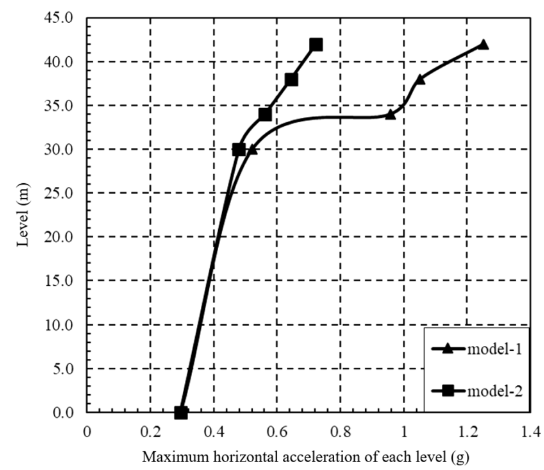

Fig. 16 Maximum horizontal acceleration of three-story flexible base models (model 1 and model 2)

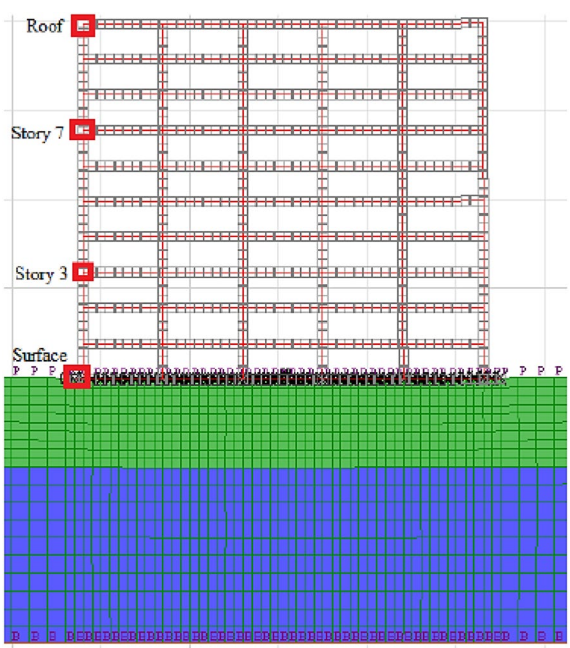

Fig. 15 Specified points of nine-story models Position to calculate the maximum horizontal acceleration (models 3, 4)

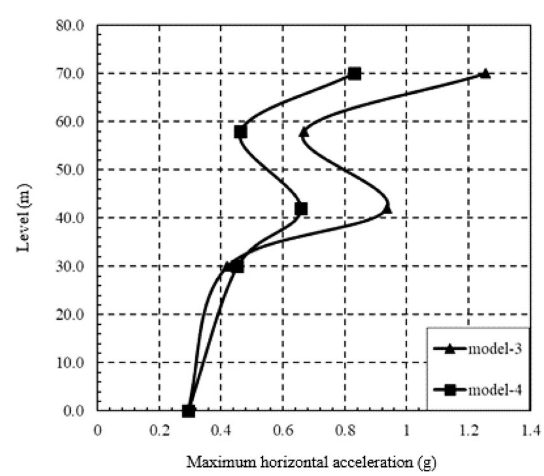

Fig. 17 Maximum horizontal acceleration of nine-story flexible base models (model 3 and model 4)

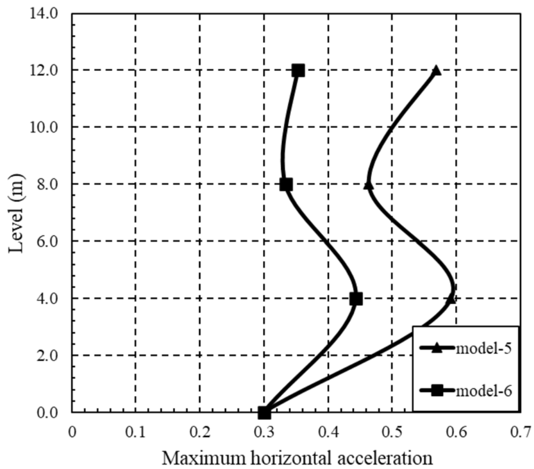

Fig. 18 Maximum horizontal acceleration of three-story fixed-base models (model 5 and model 6)

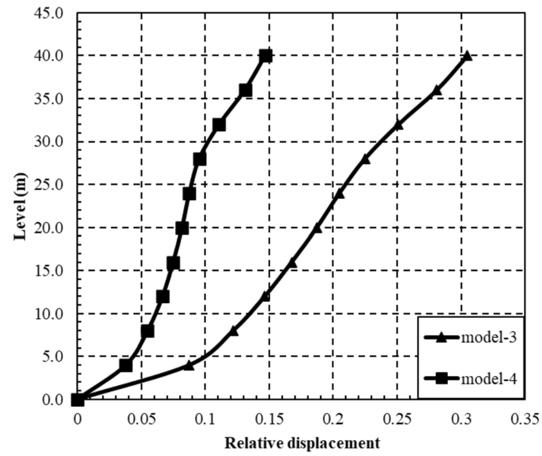

Fig. 21 Relative displacement of nine-story flexible base models (model 3 and model 4)

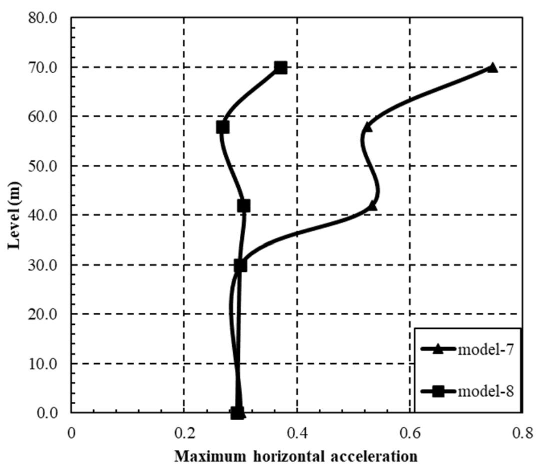

Fig. 19 Maximum horizontal acceleration of nine-story fixed-base models (model 7 and model 8)

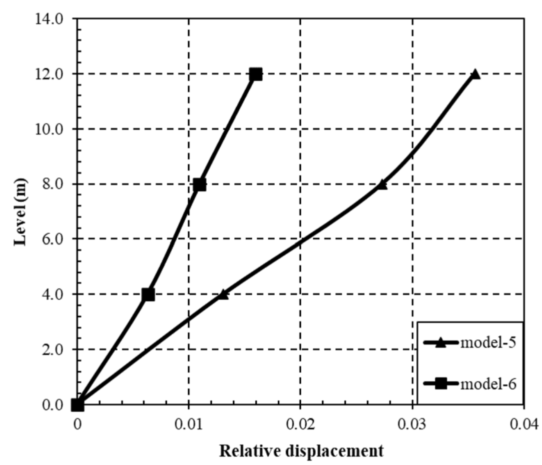

Fig. 22 Relative displacement of three-story fixed-base models (model 5 and model 6)

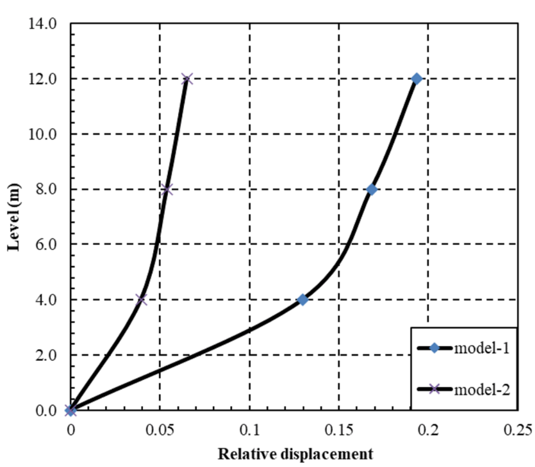

Fig. 20 Relative displacement of three-story flexible base models (model 1 and model 2)

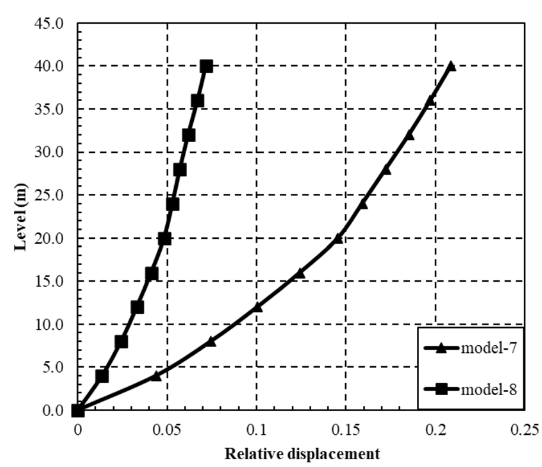

Fig. 23 Relative displacement of nine-story fixed-base models (model 7 and model 8)

Table 6 Maximum horizontal acceleration of three-story flexible base models (model 1 and model 2)

	Seismic type	Model number	Level				
			Base (g)	Surface (g)	Story 1 (g)	Story 2 (g)	Roof (g)
Three-story flexible-base models	Near fault	Model 1	0.30	0.52	0.96	1.05	1.25
	Far fault	Model 2	0.29	0.48	0.56	0.64	0.72

Table 7 Maximum horizontal acceleration of nine-story flexible base models (model 3 and model 4)

	Seismic type	Model number	Level				
			Base (g)	Surface (g)	Story 3 (g)	Story 7 (g)	Roof (g)
Nine-story flexible-base models	Near fault	Model 3	0.29	0.42	0.94	0.67	1.26
	Far fault	Model 4	0.26	0.45	0.66	0.46	0.83

Table 8 Maximum horizontal acceleration of three-story fixed-base models (model 5 and model 6)

	Seismic type	Model number	Level			
			Base (g)	Story 1 (g)	Story 2 (g)	Roof (g)
Three-story fixed-base models	Near fault	Model 5	0.3	0.59	0.46	0.57
	Far fault	Model 6	0.3	0.44	0.33	0.35

Table 9 Maximum horizontal acceleration of nine-story fixed-base models (model 7 and model 8)

	Seismic type	Model number	Level			
			Base (g)	Surface (g)	Story 3 (g)	Story 7 (g)
Three-story fixed-base models	Near fault	Model 7	0.3	0.26	0.21	0.34
	Far fault	Model 8	0.3	0.48	0.54	0.72

The nine-story building subjected to near-field motion has higher shear base results than the low-rise building, while the shear base due to far-field excitation did not significantly affect by the structure's height. Relative horizontal displacement, maximum bending moment, shear force, and axial force for the nine-story are higher than the three-story structure. The

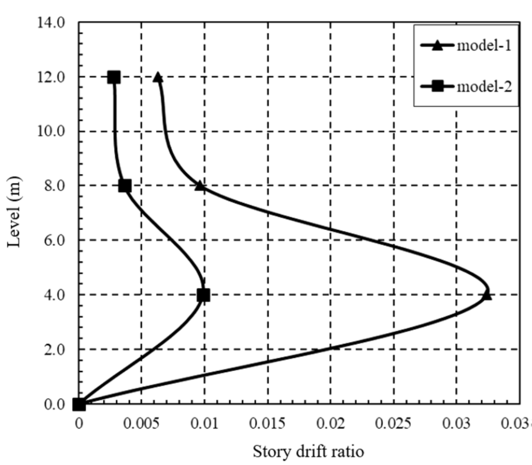

Fig. 24 Story drift ratio of three-story flexible base models (model 1 and model 2)

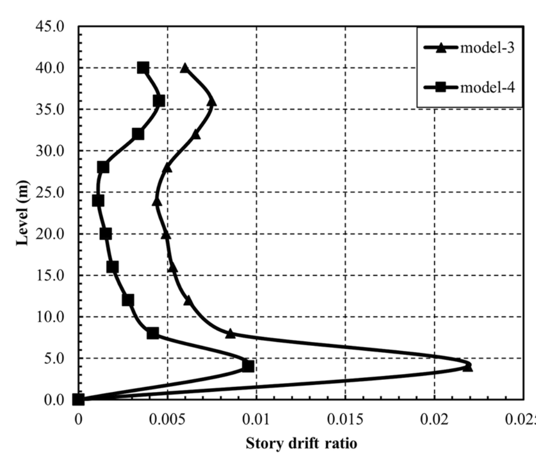

Fig. 25 Story drift ratio of nine-story flexible base models (model 3 and model 4)

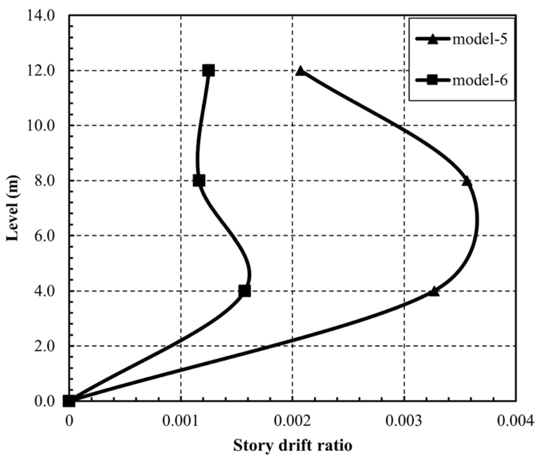

Fig. 26 Story drift ratio of three-story fixed-base models (model 5 and model 6)

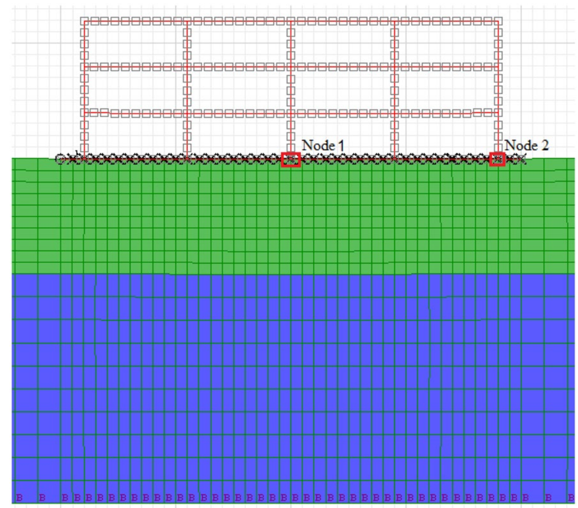

Fig. 28 Specified points of three-story flexible base models position to calculate the differential settlement

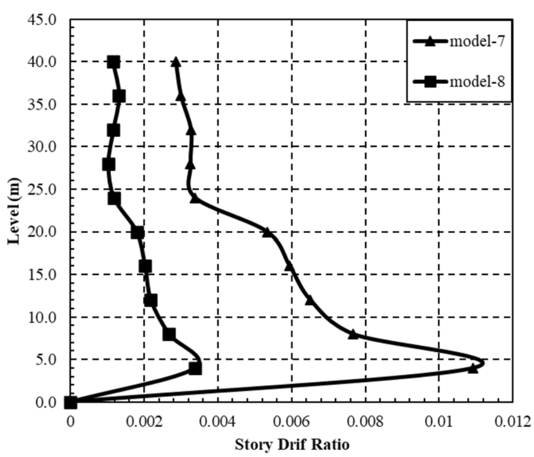

Fig. 27 Story drift ratio of nine-story fixed-base models (model 7 and model 8)

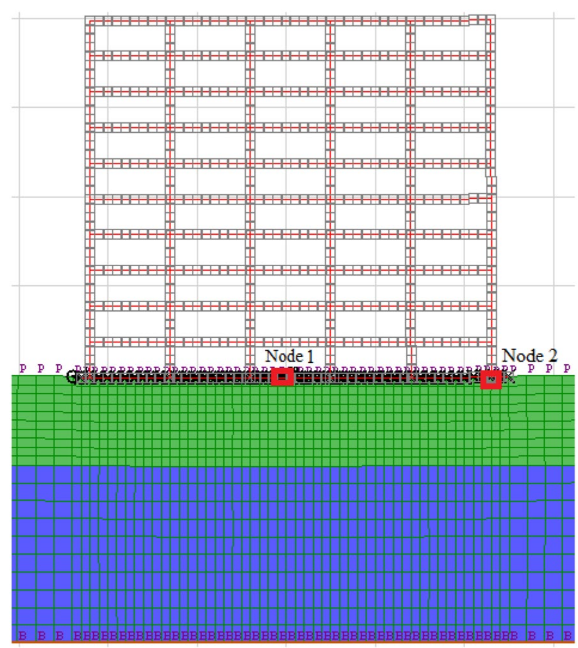

Fig. 29 Specified points of nine-story flexible base models position to calculate the differential settlement

Table 10 Comparison of settlement in flexible base models

	Seismic type	Model number	Settlement (m)
Three-story flexible-base models	Near fault	Model 1	0.04024
	Far fault	Model 2	0.03668
Nine-story flexible-base models	Near fault	Model 3	0.02677
	Far fault	Model 4	0.02358

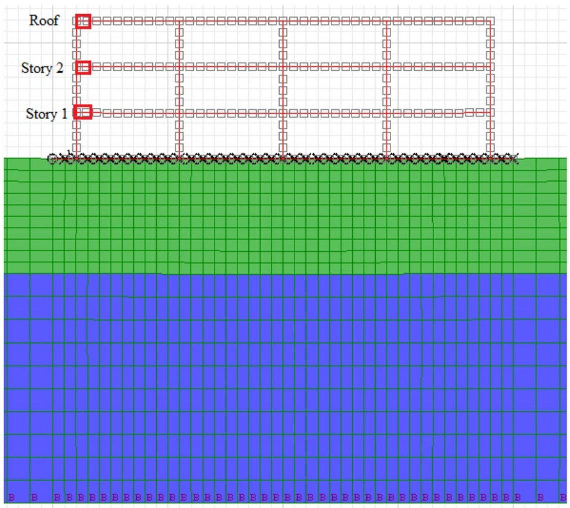

Fig. 30 Specified points of the three-story model's position to calculate the maximum bending moment and shear force

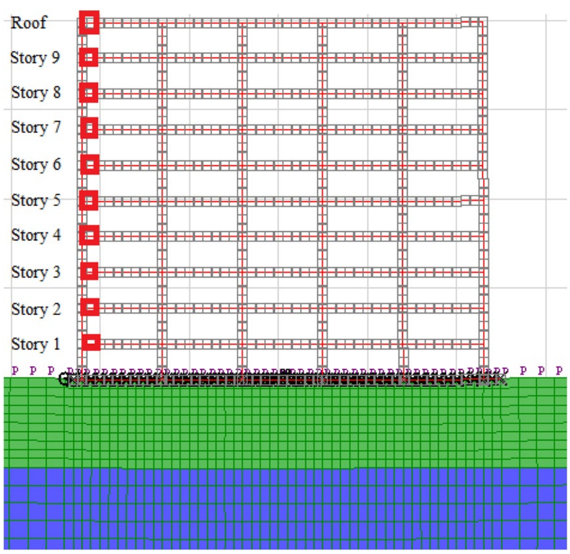

Fig. 31 Specified points of the nine-story model's position to calculate the maximum bending moment and shear force

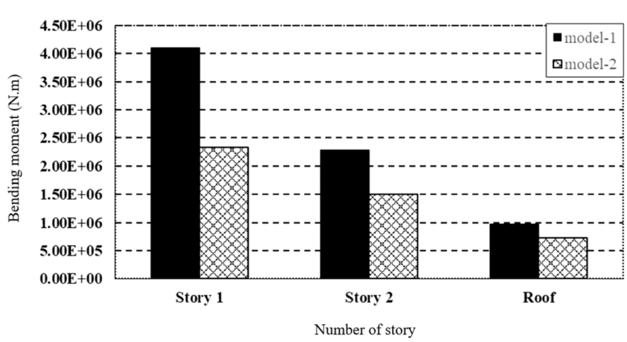

Fig. 32 Bending moment of three-story flexible base models (model 1 and model 2)

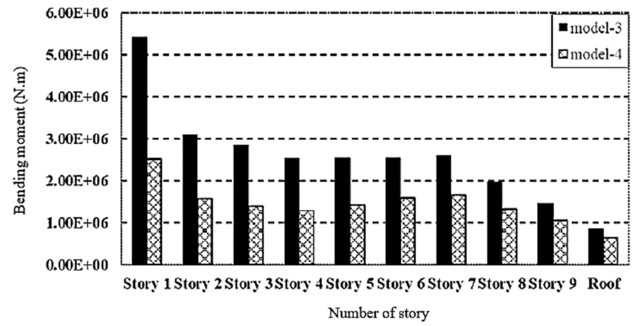

Fig. 33 Bending moment of nine-story flexible base models (model 3 and model 4)

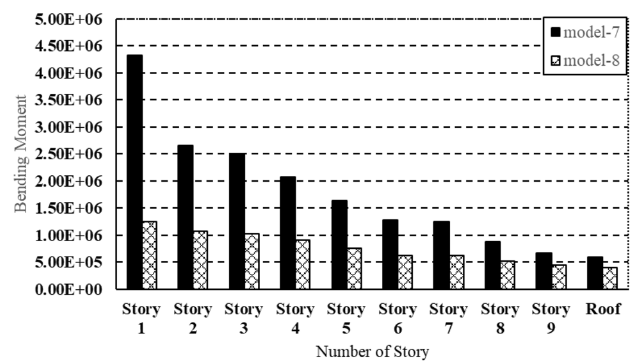

Fig. 35 Bending moment of nine-story fixed-base models (model 7 and model 8)

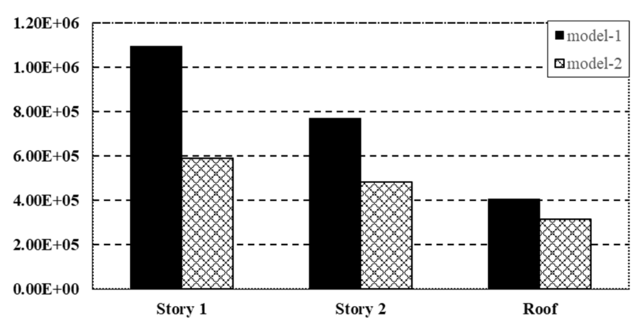

Fig. 34 Bending moment of three-story fixed-base models (model 5 and model 6)

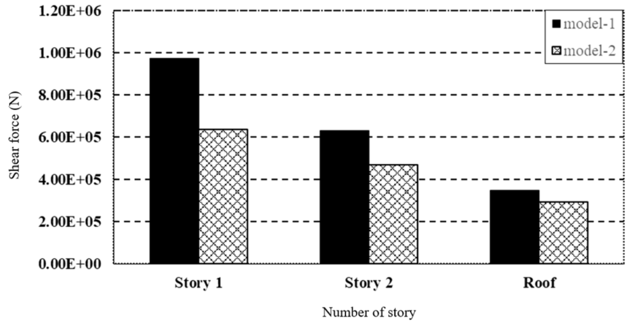

Fig. 36 The shear force of three-story flexible base models (model 1 and model 2)

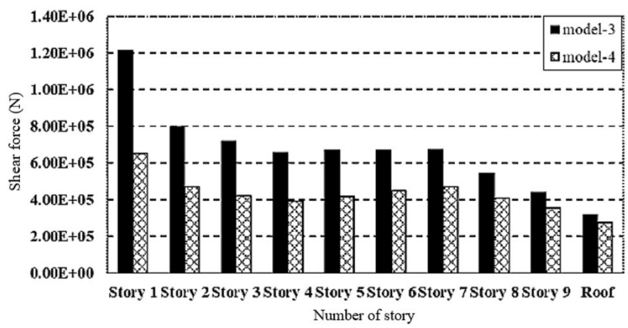

Fig. 37 The shear force of nine-story flexible base models (model 3 and model 4)

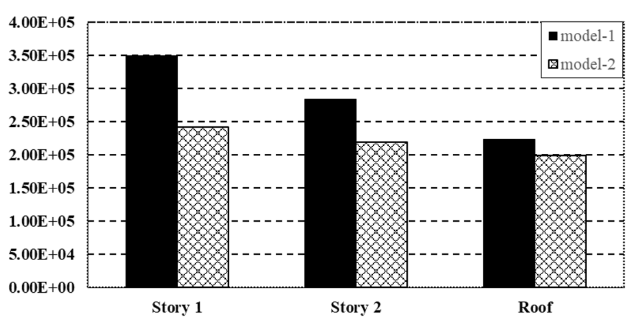

Fig. 38 The shear force of three-story fixed-base models (model 5 and model 6)

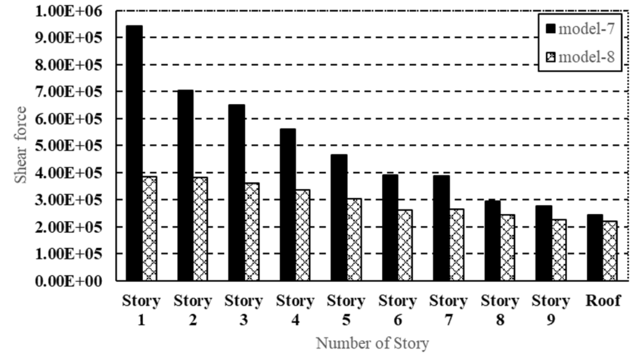

Fig. 39 The shear force of nine-story fixed-base models (model 7 and model 8)

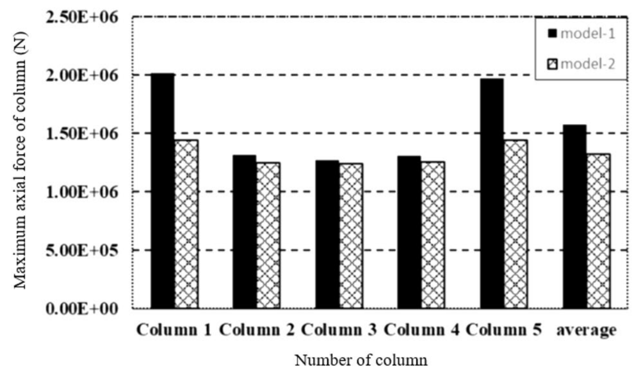

Fig. 40 The maximum axial force of columns of three-story flexible base models (model 1 and model 2)

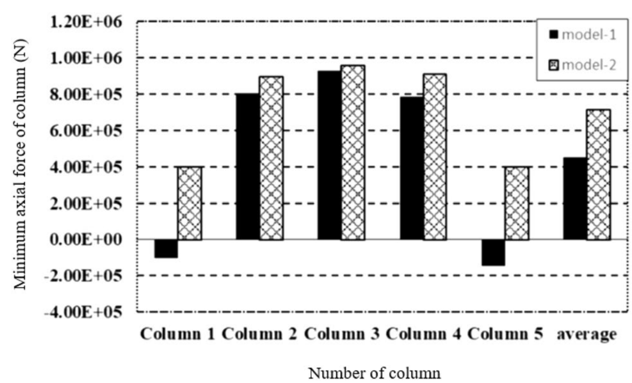

Fig. 41 The minimum axial force of columns of three-story flexible base models (model 1 and model 2)

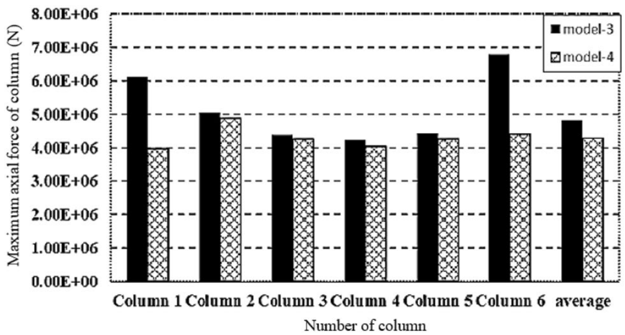

Fig. 42 The maximum axial force of columns of nine-story flexible base models (model 3 and model 4)

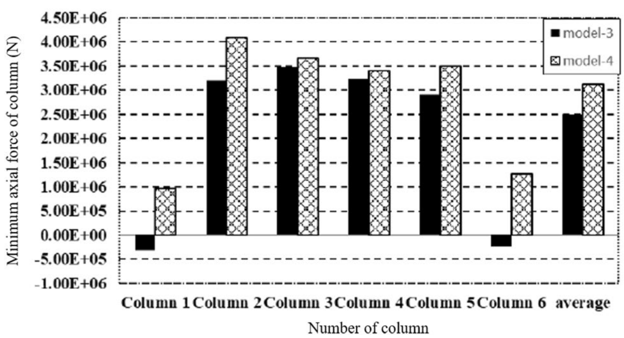

Fig. 43 The minimum axial force of columns of nine-story flexible base models (model 3 and model 4)

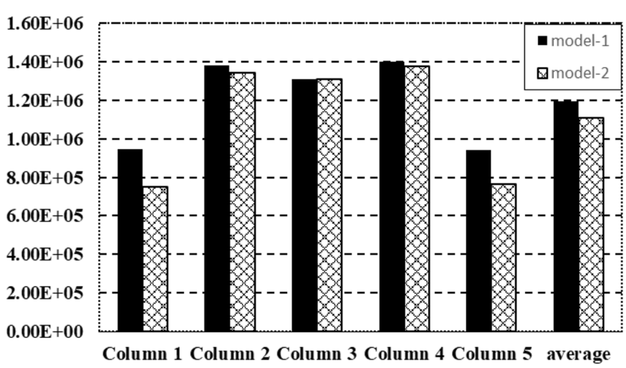

Fig. 44 The maximum axial force of columns of three-story fixed-base models (model 5 and model 6)

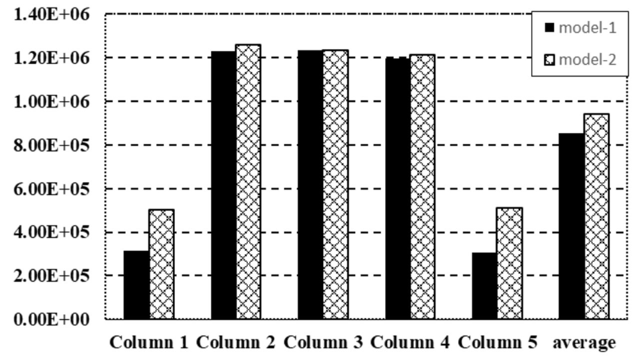

Fig. 45 The minimum axial force of columns of three-story fixed-base models (model 5 and model 6)

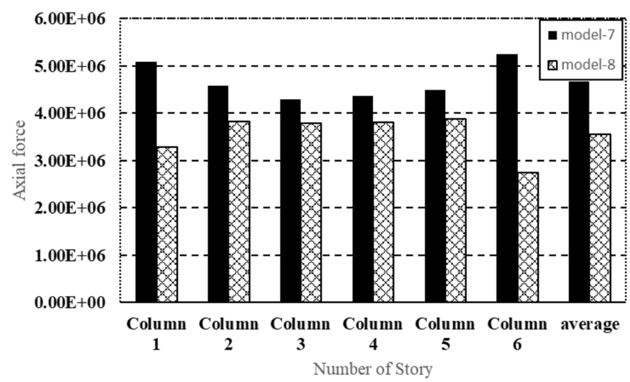

Fig. 46 The maximum axial force of columns of nine-story fixed-base models (model 7 and model 8)

maximum bending moments and shear force have higher values for the first floors compared to the upper floors of buildings and decrease by increasing the number of floors.

Supplementary Information The online version contains supplementary material available at https://doi.org/10.1007/s42107-022-00548-3.

Funding The author received no financial support for this article.

Data availability The data supporting this study's findings are available from the corresponding author upon reasonable request.

Declarations

Competing interests The authors declare that they have no conflict of interest.

References

Abd-Elhamed, A., & Mahmoud, S. (2019). Simulation analysis of TMD controlled building subjected to far- and near-fault records considering soil–structure interaction. *Journal of Building Engineering*. https://doi.org/10.1016/j.jobe.2019.100930

Adanur, S., Altunişik, A. C., Bayraktar, A., & Akköse, M. (2012). Comparison of near-fault and far-fault ground motion effects on geometrically non-linear earthquake behavior of suspension bridges. *Natural Hazards, 64*(1), 593–614. https://doi.org/10.1007/s11069-012-0259-5

Avilés, J., & Pérez-Rocha, L. E. (1998). Site effects and soil–structure interaction in the Valley of Mexico. *Soil Dynamics and Earthquake Engineering, 17*(1), 29–39.

Beheshti Aval, S. B., Mohsenian, V., & Sadegh Kouhestani, H. (2018). Seismic performance-based assessment of tunnel form building subjected to near- and far-fault ground motions. *Asian Journal of Civil Engineering, 19*(1), 79–92. https://doi.org/10.1007/s42107-018-0009-4

Bhandari, M., Bharti, S. D., Shrimali, M. K., & Datta, T. K. (2019). Seismic fragility analysis of base-isolated building frames excited by near-and far-field earthquakes. *Journal of Performance of Constructed Facilities, 33*(3), 4019029.

Bilgin, H., & Hysenlliu, M. (2020). Comparison of near and far-fault ground motion effects on low and mid-rise masonry buildings. *Journal of Building Engineering, 30*(October 2019), 101248. https://doi.org/10.1016/j.jobe.2020.101248

Bray, J. D., & Rodriguez-Marek, A. (2004). Characterization of forward-directivity ground motions in the near-fault region. *Soil Dynamics and Earthquake Engineering, 24*(11), 815–828. https://doi.org/10.1016/J.SOILDYN.2004.05.001

Chopra, A. K., & Chintanapakdee, C. (2001). Comparing response of SDF systems to near-fault and far-fault earthquake motions in the context of spectral regions. *Earthquake Engineering and Structural Dynamics, 30*(12), 1769–1789. https://doi.org/10.1002/eqe.92

Comartin, C., Niewiarowski, R., & Rojahn, C. (1996). ATC-40 seismic evaluation and retrofit of concrete buildings. *SSC 96, 1*, 1.

Conniff, D. E., & Kiousis, P. D. (2007). Elastoplastic medium for foundation settlements and monotonic soil–structure interaction under combined loadings. *International Journal for Numerical and Analytical Methods in Geomechanics, 31*(6), 789–807. https://doi.org/10.1002/nag.556

Council, B. S. S. (2003). *NEHRP recommended provisions for seismic regulations for new buildings and other structures*. Rep. No. FEMA (Vol. 450).

Davoodi, M., Jafari, M. K., & Hadiani, N. (2013). Seismic response of embankment dams under near-fault and far-field ground motion excitation. *Engineering Geology, 158*, 66–76. https://doi.org/10.1016/J.ENGGEO.2013.02.008

Dutta, S. C., Bhattacharya, K., & Roy, R. (2004). Response of low-rise buildings under seismic ground excitation incorporating soil–structure interaction. *Soil Dynamics and Earthquake Engineering, 24*(12), 893–914. https://doi.org/10.1016/J.SOILDYN.2004.07.001

Elwi, M., Muhammed, B., & Alhussiny, N. (2018). Evaluation of soil–structure interaction for structures subjected to earthquake loading with different types of foundation. *MATEC Web of Conferences, 162*, 4026.

Gerami, M., & Abdollahzadeh, D. (2015). Vulnerability of steel moment-resisting frames under effects of forward directivity. *Structural Design of Tall and Special Buildings, 24*(2), 97–122. https://doi.org/10.1002/tal.1156

Güllü, H., & Karabekmez, M. (2017). Effect of near-fault and far-fault earthquakes on a historical masonry mosque through 3D dynamic soil–structure interaction. *Engineering Structures, 152*, 465–492. https://doi.org/10.1016/j.engstruct.2017.09.031

Hardin, B. O., & Drnevich, V. P. (1972). Shear modulus and damping in soils: Design equations and curves. *Journal of the Soil Mechanics and Foundations Division, 98*(7), 667–692. https://doi.org/10.1061/JSFEAQ.0001760

Hosseinzadeh, N., Davoodi, M., & Rayat Roknabadi, E. (2012). Shake table study of soil structure interaction effects in surface and embedded foundations. In *The 15th world conference on earthquake engineering* (pp. 24–28).

Huang, X., Zhou, Z., Wang, Y., Yang, L., & Wang, Y. (2021). Structural analyses of self-centring-beam moment-frames under near-fault and far-field earthquakes. *Soil Dynamics and Earthquake Engineering, 145*(March), 106741. https://doi.org/10.1016/j.soildyn.2021.106741

Itasca Consulting Group, Inc. (2019). *FLAC3D—fast Lagrangian analysis of continua in three-dimensions, ver. 7.0*. Minneapolis: Itasca.

Khazaei, J., Amiri, A., & Khalilpour, M. (2017). Seismic evaluation of soil–foundation–structure interaction: Direct and cone model. *Earthquakes and Structures, 12*(2), 251–262.

Kramer, S. L. (1996). *Geotechnical earthquake engineering*. London: Prentice-Hall.

Kuhlemeyer, R. L., & Lysmer, J. (1973). Finite element method accuracy for wave propagation problems. *Journal of Soil Mechanics and Foundation Division, 99*(5), 421–427.

Likitlersuang, S., Surarak, C., Wanatowski, D., Oh, E., & Balasubramaniam, A. (2013). Finite element analysis of a deep excavation: A case study from the Bangkok MRT. *Soils and Foundations, 53*(5), 756–773.

Longarini, N., & Zucca, M. (2014). A Chimney's seismic assessment by a tuned mass damper. *Engineering Structures, 79*, 290–296. https://doi.org/10.1016/J.ENGSTRUCT.2014.05.020

Mansouri, I., Shahbazi, S., Hu, J. W., & Moghaddam, S. A. (2019). Effects of pulse-like nature of forward directivity ground motions on the seismic behavior of steel moment frames. *Earthquakes and Structures, 17*, 1–15.

Mashayekhi, A. H., Gerami, M., & Siahpolo, N. (2019). Assessment of higher modes effects on steel moment resisting structures under near-fault earthquakes with forward directivity effect along strike-parallel and strike-normal components. *International Journal of Steel Structures, 19*(5), 1543–1559. https://doi.org/10.1007/s13296-019-00229-z

Miranda, J. C. (2013). A method for tuning tuned mass dampers for seismic applications. *Earthquake Engineering and Structural Dynamics, 42*(7), 1103–1110. https://doi.org/10.1002/eqe.2271

Ohtori, Y., Christenson, R. E., Spencer, B. F., Jr., & Dyke, S. J. (2004). Benchmark control problems for seismically excited non-linear buildings. *Journal of Engineering Mechanics, 130*(4), 366–385.

Peer Ground Motion Data Base. (2022). https://ngawest2.berkeley.edu/

Pitilakis, D., & Karatzetzou, A. (2012). Performance-based design of soil–foundation–structure systems. In *Proceedings of the 15th world conference on earthquake engineering, Lisbon, Portugal*.

Raychowdhury, P. (2009). Effect of soil parameter uncertainty on seismic demand of low-rise steel buildings on dense silty sand. *Soil Dynamics and Earthquake Engineering, 29*(10), 1367–1378.

Rayhani, M. H., & El Naggar, M. H. (2008). Numerical modeling of seismic response of rigid foundation on soft soil. *International Journal of Geomechanics, 8*(6), 336–346. https://doi.org/10.1061/(ASCE)1532-3641(2008)8:6(336)

Reza Tabatabaiefar, H., & Fatahi, B. (2014). Idealisation of soil–structure system to determine inelastic seismic response of mid-rise building frames. *Soil Dynamics and Earthquake Engineering, 66*, 339–351. https://doi.org/10.1016/j.soildyn.2014.08.007

Sehhati, R., Rodriguez-Marek, A., ElGawady, M., & Cofer, W. F. (2011). Effects of near-fault ground motions and equivalent pulses on multi-story structures. *Engineering Structures, 33*(3), 767–779. https://doi.org/10.1016/J.ENGSTRUCT.2010.11.032

Sharma, T. K., Vijay, S., Bharti, M. K., Datta, S. (2019a). Seismic energy dissipation in semi-rigid steel frames. In *Proceedings of the 16th world conf. seism. isol. energy dissipation act. vib. control struct. proc. conf. Saint-Petersburg, July, 1–6, 2019/ ex.ed.I.I. Vedyakov;ASSISi, RAEE.Saint-Petersburg, 2019.1233*, 2019. https://doi.org/10.37153/2686-7974-2019-16

Sharma, T. K., Vijay, B., Mohit, S., Bharti, M. K., & Datta, S. D. (2022b). Seismic performance assessment of semi-rigid frames for different performance criteria. In *ISSC 2020 proceedings of the 1st Indian structural steel conference, Jan 6–8, 2022*. Indian Inst. Technol. Hyderabad, Telangana.

Sharma, T. K., Vijay, V., Sourabh, S., Bharti, M. K., Datta, S., Shrimali, S. D. B., Datta, T. K. (2019b). Energy dissipation and seismic response evaluation of semi-rigid frames at various performance levels. In *16th world conf. seism. isol. energy dissipation act. vib. control struct. proc. conf. Saint-Petersburg, July, 1–6, 2019/ex.ed.I.I. Vedyakov;ASSISi, RAEE.Saint-Petersburg*, 2019.1233 p. https://doi.org/10.37153/2686-7974-2019-16

Sharma, V., Shrimali, M. K., Bharti, S. D., & Datta, T. K. (2021). Seismic energy loss in semi-rigid steel frames under near-field earthquakes. In *Recent advances in computational mechanics and simulations* (pp. 431–443). Springer.

Sharma, V., Shrimali, M. K., Bharti, S. D., & Datta, T. K. (2022a). Seismic behavior assessment of semi-rigid frame under near-field earthquakes. In *ISSC 2020 proceedings of the 1st Indian structural steel conference, Jan 6–8, 2022*. Indian Inst. Technol. Hyderabad, Telangana.

Sharma, V., Shrimali, M., Bharti, S., & Datta, T. (2018). Behavior of mid rise semi-rigid connected steel frames under near-field and far-field earthquakes. *Paper, 1*, 1.

Sharma, V., Shrimali, M. K., Bharti, S. D., & Datta, T. K. (2020). Behavior of semi-rigid steel frames under near-and far-field earthquakes. *Steel and Composite Structures, an International Journal, 34*(5), 625–641.

Sharma, V., Shrimali, M. K., Bharti, S. D., & Datta, T. K. (2021a). Seismic demand assessment of semi-rigid steel frames at different performance points. *Steel and Composite Structures, 41*(5), 713–730.

Sharma, V., Shrimali, M. K., Bharti, S. D., & Datta, T. K. (2021b). Seismic fragility evaluation of semi-rigid frames subjected to near-field earthquakes. *Journal of Constructional Steel Research, 176*, 106384.

Somerville, P. G. (2003). Magnitude scaling of the near fault rupture directivity pulse. *Physics of the Earth and Planetary Interiors, 137*(1), 201–212. https://doi.org/10.1016/S0031-9201(03)00015-3

Stewart, J. P., Fenves, G. L., & Seed, R. B. (1999). Seismic soil–structure interaction in buildings. I: Analytical methods. *Journal of Geotechnical and Geoenvironmental Engineering, 125*(1), 26–37.

Sun, J. I., Golesorkhi, R., & Seed, H. B. (1988). *Dynamic moduli and damping ratios for cohesive soils*. University of California Berkeley.

Surarak, C., Likitlersuang, S., Wanatowski, D., Balasubramaniam, A., Oh, E., & Guan, H. (2012). Stiffness and strength parameters for hardening soil model of soft and stiff Bangkok clays. *Soils and Foundations, 52*(4), 682–697.

Van Cao, V., & Ronagh, H. R. (2014). Correlation between seismic parameters of far-fault motions and damage indices of low-rise reinforced concrete frames. *Soil Dynamics and Earthquake Engineering, 66*, 102–112. https://doi.org/10.1016/J.SOILDYN.2014.06.020

Warnitchai, P., Sangarayakul, C., Ashford, S. A. (2000). Seismic hazard in Bangkok due to long-distance earthquakes. In *Proceedings of the 12th world conference on earthquake engineering (Vol. 30), Auckland, New Zealand*.

Xie, W., & Sun, L. (2021). Experimental and numerical investigations on transverse seismic responses of soil-cable-stayed-bridge system subjected to transverse near-fault ground motions. *Engineering Structures, 226*, 111361. https://doi.org/10.1016/J.ENGSTRUCT.2020.111361

Zhang, S., & Wang, G. (2013). Effects of near-fault and far-fault ground motions on non-linear dynamic response and seismic damage of concrete gravity dams. *Soil Dynamics and Earthquake Engineering, 53*, 217–229. https://doi.org/10.1016/j.soildyn.2013.07.014

Zhang, Z., & Balendra, T. (2013). Passive control of bilinear hysteretic structures by tuned mass damper for narrow band seismic motions. *Engineering Structures, 54*, 103–111. https://doi.org/10.1016/J.ENGSTRUCT.2013.03.044

Zomorodian, R., Soltani, F., Sivandi-Pour, A., & Farsangi, E. N. (2021). Effect of foundation flexibility on the seismic performance of a high-rise structure under far-field and near-field earthquakes. *International Journal of Engineering, Transactions a: Basics, 34*(7), 1611–1622. https://doi.org/10.5829/IJE.2021.34.07A.06